

Article

Effect of SnO₂ Colloidal Dispersion Solution Concentration on the Quality of Perovskite Layer of Solar Cells

Keke Song¹, Xiaoping Zou^{2,*}, Huiyin Zhang^{1,*}, Chunqian Zhang², Jin Cheng², Baoyu Liu¹, Yujun Yao², Xiaolan Wang², Xiaotong Li², Yifei Wang² and Baokai Ren²

¹ School of Instrument Science and Opto Electronics Engineering, Beijing Information Science and Technology University, Beijing 100101, China; songmengke163@163.com (K.S.); liubaoyu0214@163.com (B.L.)

² Beijing Advanced Innovation Center for Materials Genome Engineering, Beijing Key Laboratory for Sensor, Beijing Information Science and Technology University, Beijing 100101, China; chunqiancool@163.com (C.Z.); chengjin@bistu.edu.cn (J.C.); yyj10zy@gmail.com (Y.Y.); wangxl1105@163.com (X.W.); xiaotong252240@163.com (X.L.); yifeiwang2020@126.com (Y.W.); renbk2021@163.com (B.R.)

* Correspondence: xpzou2020@bistu.edu.cn or xpzou2014@163.com (X.Z.); zhy@bistu.edu.cn (H.Z.); Tel.: +86-1364-105-6404 (X.Z.); +86-1860-084-3626 (H.Z.)

Abstract: The electron transport layer (ETL) is critical to carrier extraction for perovskite solar cells (PSCs). Moreover, the morphology and surface condition of the ETL could influence the topography of the perovskite layer. ZnO, TiO₂, and SnO₂ were widely investigated as ETL materials. However, TiO₂ requires a sintering process under high temperature and ZnO has the trouble of chemical instability. SnO₂ possesses the advantages of low-temperature fabrication and high conductivity, which is critical to the performance of PSCs prepared under low temperature. Here, we optimized the morphology and property of SnO₂ by modulating the concentration of a SnO₂ colloidal dispersion solution. When adjusting the concentration of SnO₂ colloidal dispersion solution to 5 wt.% (in water), SnO₂ film indicated better performance and the perovskite film has a large grain size and smooth surface. Based on high efficiency (16.82%), the device keeps a low hysteresis index (0.23).

Keywords: perovskite solar cell; electron transport layer; SnO₂ colloidal dispersion solution; the low temperature



Citation: Song, K.; Zou, X.; Zhang, H.; Zhang, C.; Cheng, J.; Liu, B.; Yao, Y.; Wang, X.; Li, X.; Wang, Y.; et al. Effect of SnO₂ Colloidal Dispersion Solution Concentration on the Quality of Perovskite Layer of Solar Cells. *Coatings* **2021**, *11*, 591. <https://doi.org/10.3390/coatings11050591>

Academic Editor: Alicia de Andrés

Received: 21 March 2021

Accepted: 14 May 2021

Published: 18 May 2021

Publisher's Note: MDPI stays neutral with regard to jurisdictional claims in published maps and institutional affiliations.



Copyright: © 2021 by the authors. Licensee MDPI, Basel, Switzerland. This article is an open access article distributed under the terms and conditions of the Creative Commons Attribution (CC BY) license (<https://creativecommons.org/licenses/by/4.0/>).

1. Introduction

ETLs in PSCs not only promote the separation of photogenerated electron-hole pairs but also improves the charge transport efficiency, thus avoiding the influence of charge accumulation on the device lifetime. At the same time, the material of ETL could significantly affect the topography of perovskite layers and device performance [1–5]. Our widely applied ETL materials are organic and inorganic materials. Although organic materials have good solubility in the treatment process, their low electron mobility and high cost hinder the commercialization of PSCs. Inorganic materials, especially metal oxides [6–18], are endowed with superior advantages of low cost, high stability, and excellent photoelectric property [12,19,20], are usually used as electron transport layer materials.

Metal oxides such as TiO₂ [6–9], ZnO [14,15], and SnO₂ [10–14,21], have become the mainstream materials of ETLs. Giordano and co-workers have demonstrated that the electronic trap states could be reduced and electron transport could be enhanced by introducing Li-ions into TiO₂ ETLs [22]. Finally, the power conversion efficiency (PCE) rocketed to 19% from 17%. However, the mesoporous TiO₂ ETL requires a sintering process under high temperature, which limits the development of low-temperature and high-efficiency solar cells. Furthermore, PSCs prepared under low-temperature have aroused great interest in the past ten years. Ding and co-workers have prepared perovskite thin film with full coverage, high density, and good uniformity by increasing crystallizing speed on the ZnO electron transport layer [23]. However, the ZnO is not stable due to

its chemical properties and the interface between ZnO and perovskite could degrade at high temperature, which demonstrates that ZnO ETL is not desirable for PSCs. However, SnO₂ has high electron mobility and high transparency [24]. Comparatively, SnO₂ has high electron mobility (10^{-2} μS/cm) and a high conductivity (10^1 cm² V⁻¹ S⁻¹), as shown in Table S1 (Supplementary Materials). Therefore, SnO₂ is critical to the performance of PSCs prepared under low temperature.

The SnO₂ colloidal dispersion solution concentration used to prepare ETL has a significant effect on the perovskite film quality. Li et al. [25] reported that the high quality of ETLs can be produced by controlling the thickness of the film while it is treated by UV. The thickness is dependent on the concentration of SnO₂. When the concentration of SnO₂ was 20%, the PSCs obtained an optimal performance. Yang et al. [21] reported on EDTA-complexed SnO₂ ETLs by complexing EDTA with SnO₂ in planar-type PSCs, Yang et al. [26] and Qiang et al. [27] prepared the ETL material by dispersing the as-synthetic SnO₂ in the low boiling ethanol and the concentration of the SnO₂ spin-coating solution was optimized. However, the influence of the ETL formed by different SnO₂ concentrations on the quality of the perovskite film has not been carefully studied. Bahadur and co-workers [28] demonstrated that the PSC could exhibit a PCE of 8.51% when the volume ratio of SnO₂ colloidal solution and deionized water is 1:4. Therefore, SnO₂ could be applied in planer PSCs prepared under low-temperature and humid environments as superior roll-to-roll-capable ETLs. However, few works about the quality of the perovskite layer deposited on tin dioxide ETL has been reported. Bu and co-workers [29] studied the morphology and grain size of CsFAMA perovskite deposited on Alfa-SnO₂ ETL and water Alfa-SnO₂/KOH ETLs. However, the concentration of SnO₂ colloidal dispersion was not optimized. In recent years, Huang and co-workers [30] increased the substrate transmittance and reduced the density of trap-state of the perovskite layer by using the optimized SnO₂ layer. However, the optimal concentration interval of SnO₂ was relatively large.

In this paper, we systematically studied the single cation perovskite films formed on the ETL prepared with various concentrations of SnO₂ colloidal dispersion solution at room temperature. We found that the ETL formed with SnO₂ colloidal dispersion solution of different concentrations could affect the device performance as well as perovskite film morphology. When the SnO₂ colloidal dispersion solution concentration is set to be 5 wt.%, the perovskite film exhibits high quality with a large grain size. Moreover, the device efficiency is high and hysteresis is negligible.

2. Experiments

2.1. Materials

Indium tin oxide (ITO) glass substrates, ITO polyethylene terephthalate (PET) substrates were obtained from South China Science & Technology Company Limited (Yiyang, China). N,N-dimethylformamide (DMF, 99.8%), chlorobenzene, ethanol, dimethyl sulfoxide (DMSO, 99.8%), acetone and isopropanol were bought from Sinopharm Chemical Reagent Beijing Co. Ltd. (Beijing, China). Tin dioxide (SnO₂, Alfa Aesar, 15 wt.% in H₂O colloidal dispersion) was bought from Alfa Aesar (China) Co., Ltd. (Shanghai, China). Spiro-OMeTAD (≥99.5%), lead(II) iodide (PbI₂, 99.99%), Methyl ammonium iodide (CH₃NH₃I, MAI, >99.5%) and isopropyl alcohol (IPA) were bought from Xi'an Polyme Light Technology Corp. (Xi'an, China). Deionized water was prepared by Beijing Key Laboratory for Sensor, Beijing Information Science and Technology University (Beijing, China).

2.2. Device Fabrication

2.2.1. ITO Substrate Cleaning Process

First, ITO substrate (PET/ITO and Glass/ITO) were cleaned with deionized water and detergent of suitable ratio in ultrasonic cleaner for 20 min. The ultrasonic cleaner was bought from Skymen Cleaning Technology Shenzhen Co., Ltd. The cleaner was manufactured in Shenzhen, China and the machine model is KQ-100E. Secondly, the processed ITO was treated with ethanol for twenty minutes in the ultrasonic cleaner.

Thirdly, the ITO was treated with the mixed solvents of isopropyl alcohol, acetone, and deionized water for twenty minutes in the ultrasonic cleaner. The volume ratio of isopropyl alcohol, acetone and deionized water is 1:1:1. Finally, the ITO was treated with UV light for fifteen minutes in UV light cleaner, removing the organics. The UV light cleaner was purchased from Shenzhen Huiwo Technology Co., Ltd. The model was BZS250GF-TC and the machine was manufactured in Shenzhen, China.

2.2.2. Electron Transport Layer (ETL) Preparing Process

SnO₂ ETL has been formed by spin-coating the diluted SnO₂ colloidal solution at 3000 rpm/s for thirty seconds. Then the film was annealed at 150 degrees Celsius for thirty minutes. It is worth noting that the SnO₂ colloidal solution was diluted from an initial 20 wt.% concentration, which was confirmed to be the accurate concentration (though the label concentration was 15 wt.%) [12]. Specifically, the diluting volume ratios (pristine SnO₂ colloidal solution: H₂O) for 10, 6.67, 5, 4, and 3.33 wt.% SnO₂ precursors were 1:1, 1:2, 1:3, 1:4, and 1:5, respectively.

2.2.3. Perovskite Absorption Layer Preparing Process

DMSO and DMF were used to disperse the PbI₂ powder to make 600 mg/mL precursor solution. The volume ratio of DMSO and DMF is 0.05:0.95. The CH₃NH₃I was dispersed in isopropyl alcohol to make the precursor solution. The precursor solution concentration is 70 mg/mL. Secondly, the lead diiodide layer was formed on the SnO₂ film by spin-coating lead diiodide precursor solution. The speed is 1500 rpm/s and the time is thirty seconds. Next, the perovskite layer was formed by spin-coating CH₃NH₃I precursor solution on the as-formed PbI₂ layer. The speed is 1500 rpm/s and the time is thirty seconds. Finally, the film was annealed at 150 degrees Celsius for twenty minutes.

2.2.4. Hole Transport Layer (HTL) Preparing Process

First, 5 mL of acetonitrile solution has been used to disperse 260 mg of Li-TFST. Then, 2 mL of chlorobenzene solution has been used to disperse 35 µL of TBP and 14.46 mg of Spiro-OMeTAD powder. The Spiro-OMeTAD precursor solution was finally formed by mixing the two solutions together. The HTL was made by spin-coating the prepared precursor solution on perovskite substrate. The speed is 3000 rpm/s and the time is thirty seconds. and annealing the as-formed film at sixty degrees Celsius for five minutes. Finally, the Spiro-OMeTAD layer was treated with oxidization for ten hours at ambient atmosphere.

2.2.5. Counter Electrode Preparation Process

The samples prepared by each layer were put into the vacuum thermal evaporation coating equipment to begin the preparation of the gold electrode. The gold (Au) electrode was prepared with a thermal vapor deposition method in high vacuum environment. The device area was defined by the overlap of ITO electrode and Au electrode, which was 0.2 cm × 0.2 cm.

2.3. Characterization

The morphological images of perovskite films were obtained with scanning electron microscope (SEM, Zeiss SIGMA, Kanagawa, Japan). A solar simulator equipped with air-mass (AM) 1.5 sunlight has been applied to conduct J–V test. The solar simulator model is Sol 3A and the machine is manufactured in Oriel, Newport, RI, USA. X-ray diffractometer was applied to obtain X-ray diffraction (XRD, D8 Focus, Bruker, Dresden, Germany) data of perovskite films formed on ITO/SnO₂ substrates. All the measurements are conducted in ambient conditions.

3. Results and Discussion

We have investigated the effects of different SnO₂ colloidal dispersion solution concentrations on perovskite films and the scanning electron microscope (SEM) measurements

were performed. Figure 1 demonstrates the top-view SEM images of the perovskite layers spin-coated on an SnO₂ layer of different colloidal dispersion solution concentrations. As demonstrated in Figure 1a, the SnO₂ colloidal dispersion solution concentration was 10 wt.%, some holes appeared on the surface of perovskite. When the colloidal dispersion solution concentration of SnO₂ was 6.67 wt.% (Figure 1b), the holes on the surface of perovskite layer were significantly reduced. As shown in Figure 1d,e, when the SnO₂ colloidal dispersion concentration solution was 4 wt.% and 3.33 wt.%, Some holes appear on the surface of the perovskite and the grain size becomes larger. As demonstrated in Figure 1c, when the SnO₂ colloidal dispersion solution concentration was 5 wt.%, the perovskite film quality was significantly improved compared with the previous concentrations of 10, 6.67, 4, and 3.33 wt.%.

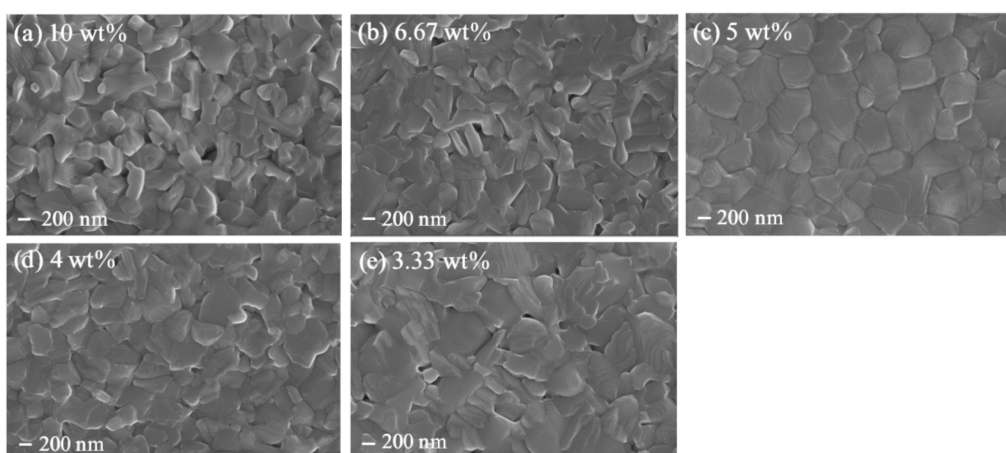


Figure 1. SEM images for the perovskite layers formed on different SnO₂ layers. SnO₂ colloid solutions of different concentrations: (a) 10 wt.%, (b) 6.67 wt.%, (c) 5 wt.%, (d) 4 wt.%, and (e) 3.33 wt.%.

From the perovskite film SEM images, we could observe that the films exhibit the best quality with larger grain size and few holes when the concentration of SnO₂ colloidal dispersion solution was 5 wt.%.

The XRD patterns for the perovskite films formed on the various SnO₂ ETLs are shown in Figure 2. The XRD patterns in Figure S1 (Supplementary Materials) showed same peak positions, which were $2\theta = 26.7^\circ$ for (100), $2\theta = 22.1^\circ$ for (110), $2\theta = 53.6^\circ$ for (211), $2\theta = 64.6^\circ$ for (310), and $2\theta = 69.5^\circ$ for (112) (JCPDS card 770452). Figure 2 shows seven intense and sharp peak positions, corresponding to (110), (200), (211), (202), (220), (310), and (312) crystal planes of perovskite, respectively [29]. The peak intensity of the (110) crystal plane of perovskite is the highest when the concentration of SnO₂ colloidal dispersion solution was 5 wt.%, this is because at the concentration the surface of SnO₂ has a certain roughness, as shown in Figure S2 (Supplementary Materials), which assists in the stress release during the annealing of the perovskite layer, resulting in a good quality of perovskite crystallization with almost no holes.

The relative intensity ratio of the PbI₂ peak and (110) of MAPbI₃ with the XRD patterns are shown in Table 1. By comparing the relative intensity ratio of the PbI₂ peak and (110) of MAPbI₃, we determined that the relative intensity ratio gradually increased with the decrease of SnO₂ colloidal dispersion solution concentrations, indicating that there was PbI₂ remaining in the perovskite layers. The reported work shows that moderate excessive PbI₂ can passivate the defects of the perovskite film [31]. When the SnO₂ colloidal dispersion solution concentration was 5 wt.%, the content of PbI₂ is relatively moderate, which indicates that the quality of perovskite layer is relatively good. This experiment result is consistent with that of SEM.

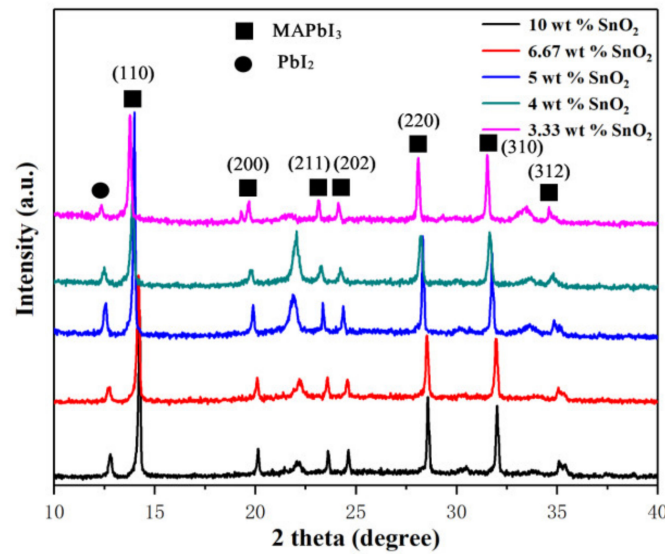


Figure 2. XRD patterns for perovskite films deposited on various SnO₂ layers.

Table 1. The relative intensity ratio of the PbI₂ peak and (110) of MAPbI₃ with XRD patterns of perovskite film.

Samples	Relative Intensity Ratio
10 wt.% SnO ₂	0.18
6.67 wt.% SnO ₂	0.43
5 wt.% SnO ₂	0.47
4 wt.% SnO ₂	0.76
3.33 wt.% SnO ₂	0.76

Figure 3 demonstrates the J–V curves for PSCs prepared with various SnO₂ colloidal dispersion solution concentrations. When the SnO₂ colloidal dispersion solution concentration is 5 wt.%, the overall performance of the device is relatively higher, especially the open-circuit voltage (V_{OC}) and short-circuit current density (J_{SC}) is much higher than those of others. Moreover, PSCs prepared with 5 wt.% SnO₂ colloidal dispersion solution have a low hysteresis index (HI) based on high efficiency.

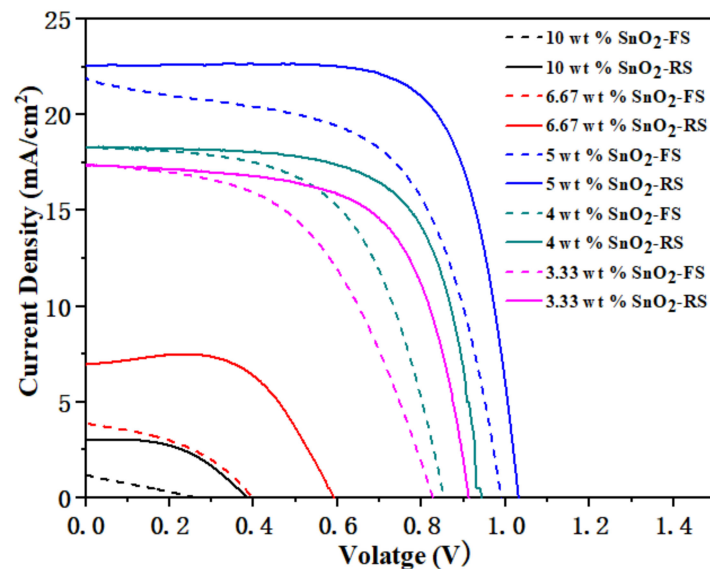


Figure 3. The current density–voltage (J–V) curves for perovskite solar cells made with SnO₂ colloid solution with different concentrations.

Table 2 shows the parameters of performance calculated from J–V curves in Figure 3. It can be seen from Table 2 that different SnO₂ colloidal dispersion solution concentrations have a significant impact on the PSC performance. When the SnO₂ colloidal dispersion concentration solution is 5 wt.%, the J_{SC} of the PSC is 22.57 mA/cm², the V_{OC} is 1.03 V, and the filling factor (FF) is 73%. On this basis, the device has relatively high PCE and low HI.

Table 2. Data of performance of PSCs prepared with SnO₂ colloid solution of different concentrations.

Samples	Scanning Direction	V _{OC} (V)	J _{SC} (mA/cm ²)	FF (%)	PCE (%)	HI
10 wt.% SnO ₂	FS	0.28	1.06	28	0.08	0.91
	RS	0.41	3.84	48	0.86	
6.67 wt.% SnO ₂	FS	0.43	4.17	24	0.43	0.83
	RS	0.59	6.96	62	2.55	
5 wt.% SnO ₂	FS	0.99	21.93	59	12.90	0.23
	RS	1.03	22.57	73	16.82	
4 wt.% SnO ₂	FS	0.85	18.31	59	9.15	0.22
	RS	0.94	18.33	68	11.71	
3.33 wt.% SnO ₂	FS	0.87	15.70	60	8.19	0.23
	RS	0.96	15.66	71	10.68	

Note: FS: Forward Scan; RS: Reverse Scan; HI = (PCE_{RS} – PCE_{FS})/PCE_{RS}.

We have obtained the statistics of PCE of PSCs to justify the effect of concentration of SnO₂ colloidal dispersion solution on the device performance (Figure 4). The data in Figure 4 represent reverse scanned data. Figure 4 demonstrates that the parameters of performance of 5 wt.% SnO₂ colloidal dispersion solution concentration-based devices exhibit relatively higher repeatability than the others.

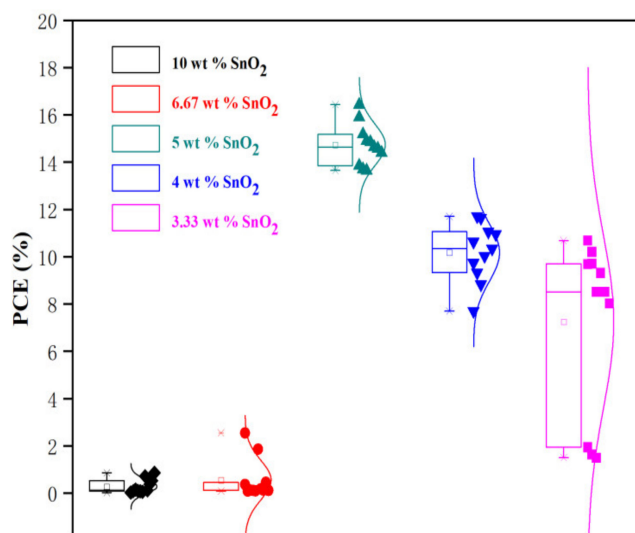


Figure 4. The statistical plots of PCE of reverse scanned data. The average value is demonstrated with the boxes. The third quartile and first quartile are demonstrated with lower and upper box boundaries, respectively. The minimum and maximum values are demonstrated with the whiskers, and the median is demonstrated with the middle line in each box. Eleven devices in each group are prepared under the same conditions.

By optimizing the ETL preparation process, we obtained a relatively good process (SnO₂ colloidal dispersion concentration of 5 wt.%). Referring to this process, we prepared a flexible perovskite solar cell (F-PSC). Figure 5 demonstrates the reverse scanning J–V curves for an F-PSC prepared under optimized conditions. Table 3 shows the parameters of device performance calculated from reverse scanning J–V curves. It can be concluded

from Table 3 that the flexible device exhibits a PCE of 7%. Based on the initial F-PSC, we made two bends with a curvature radius of 5 mm. After two bends with a curvature radius of 5 mm, the PCE is reduced to 46% of the initial F-PSC (The inset shows the photograph of F-PSC). This is caused by the brittle nature of polycrystalline perovskite layer, making the film vulnerable to damage under destructive bending experiments, which would deteriorate the device performance. However, the F-PSC can still work compared to rigid substrate-based PSCs.

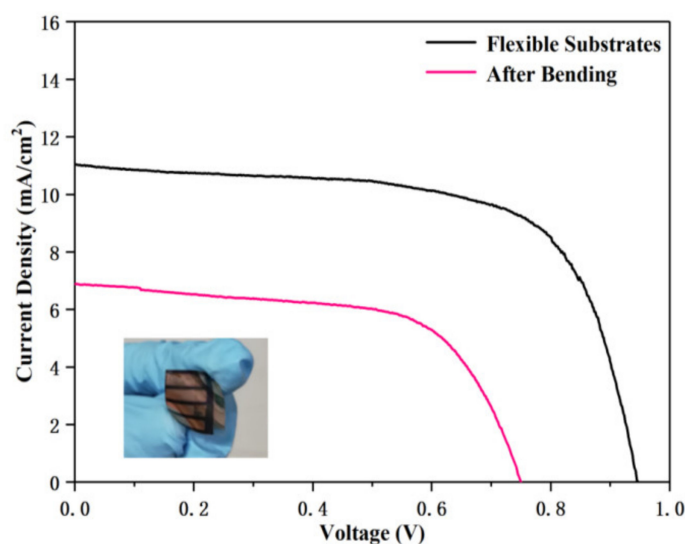


Figure 5. Reverse scanning J–V curves for pristine flexible PSC prepared with SnO₂ colloid solution of the concentration of 5 wt.% and the PSC after bending. (The illustration is the photograph of F-PSC).

Table 3. Parameters calculated from reverse scanning J–V curves for flexible PSC fabricated with SnO₂ colloid solution of the concentration of 5 wt.%.

Samples	PCE (%)	V _{OC} (V)	J _{SC} (mA/cm ²)	FF (%)
Flexible Substrate	7.00	0.95	11.03	67.00
Bending (Radius of curvature is 5 mm)	3.21	0.75	6.88	63.00

To compare the morphology of perovskite film deposited on rigid substrate (Glass/ITO) and flexible substrate (PET/ITO), we conducted the SEM characterization of the perovskite film based on the same preparation process of the flexible substrate, as shown in Figure 6. We could find that the perovskite film is uneven and the grains are small. Moreover, grain stacks can be clearly observed from Figure 6, and the quality of the perovskite film prepared is poor. Perovskite films prepared on rigid substrate (as shown in Figure 1c) exhibit a better quality than flexible substrate. We speculate that the poor quality of the flexible substrate itself, resulting in the poor perovskite film quality.

Figure 7 and Table 4 show the performance of PSCs prepared on two substrates. We could find that the PSCs prepared on rigid substrate obtained the V_{OC} of 1.03 V and the PCE of 16.82%. The F-PSC prepared on a flexible substrate (PET/ITO) by using the same preparation process exhibited the V_{OC} of 0.95 V and the PCE of 7.00%. It indicates that the quality of the perovskite layer prepared on a rigid substrate exhibits far higher than that on a flexible substrate, so the optimization of the preparation process of F-PSC remains to be studied.

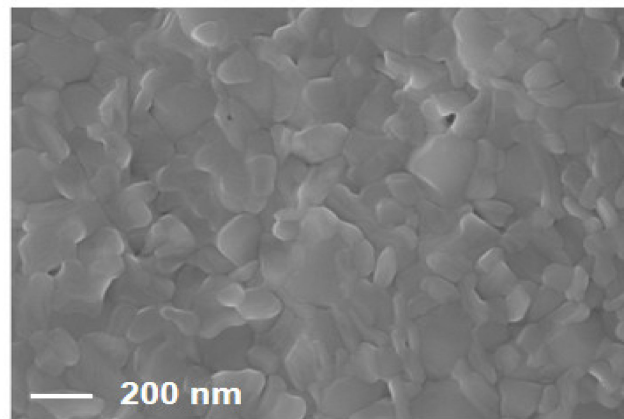


Figure 6. SEM image for perovskite layer deposited on flexible substrate.

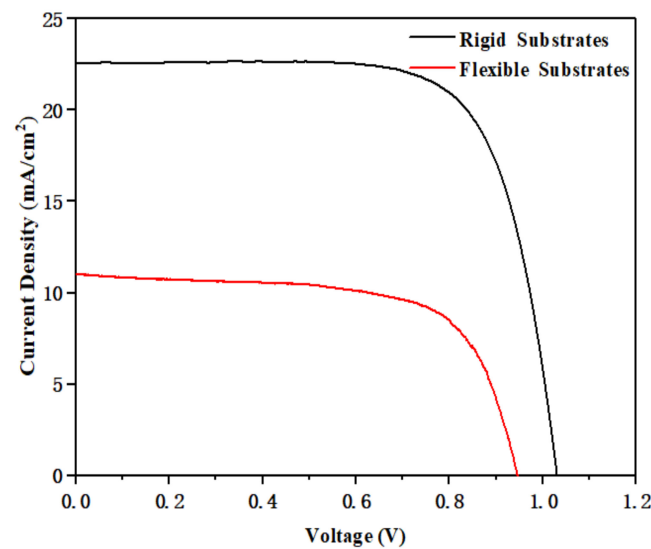


Figure 7. J–V curves for perovskite solar cells (reverse scanning) prepared on two substrates. Our concentration of SnO₂ colloid solution is 5 wt.%.

Table 4. Parameters calculated from Figure 7. Our concentration of the SnO₂ colloid solution is 5 wt.%.

Samples	PCE (%)	V _{OC} (V)	J _{SC} (mA/cm ²)	FF (%)
Rigid Substrate	16.82	1.03	22.57	73
Flexible Substrate	7.00	0.95	11.03	67

4. Conclusions

In summary, we studied the influence of the concentration of SnO₂ colloidal dispersion solution on the topography of perovskite layer and performance of PSCs. We found that the perovskite film prepared with 5 wt.% SnO₂ colloidal dispersion solution has a large grain size and the morphology of perovskite layer could be modulated by controlling the SnO₂ colloidal dispersion solution concentration. Moreover, when our SnO₂ colloidal dispersion solution concentration was 5 wt.%, the content of PbI₂ is relatively moderate. The defects of perovskite films could be passivated with suitable PbI₂ residue, which favors the performance of PSCs prepared under high temperature. The PCE and FF of the device can reach 16.82% and 73%, respectively. We also found that the HI could be modulated by adjusting the concentration of SnO₂ colloidal dispersion solution. Based on high efficiency (16.82%), the HI was relatively low (0.23) when the SnO₂ colloidal dispersion solution

concentration was 5 wt.%. Our work has provided a reference for low-temperature and high-performance optoelectronic device preparation process in the future.

Supplementary Materials: The following are available online at <https://www.mdpi.com/article/10.3390/coatings11050591/s1>, Figure S1: The XRD patterns of the original layers of SnO₂ with different concentrations of SnO₂ colloidal dispersion solution. SnO₂ colloid solution of different concentrations: (a) 10 wt.%, (b) 6.67 wt.%, (c) 5 wt.%, (d) 4 wt.%, (e) 3.33 wt.%. Figure S2: Atomic Force Microscope (AFM) of different concentrations of SnO₂ colloidal dispersion solution. The roughness of the films is recorded on the right side of the images. Table S1: Hall effect measurements of SnO₂ film.

Author Contributions: Conceptualization, X.Z. and H.Z.; Data curation, Y.Y., Y.W. and B.R.; Funding acquisition, X.Z. and H.Z.; Investigation, K.S.; Methodology, K.S., C.Z., and B.L.; Resources, C.Z., J.C., and B.L.; Supervision, X.Z., H.Z., and J.C.; Visualization, Y.Y., X.W., and X.L.; Writing—original draft, K.S.; Writing—review & editing, X.W., X.L., Y.W., and B.R. All authors have read and agreed to the published version of the manuscript.

Funding: Funding: This research was funded by the National Natural Science Foundation of China, grant numbers 61875186 and 61901009, State Key Laboratory of Advanced Optical Communication Systems Networks of China (2021GZKF002) and Beijing Key Laboratory for Sensors of BISTU (No. 2019CGKF007).

Institutional Review Board Statement: Not applicable.

Informed Consent Statement: Not applicable.

Data Availability Statement: The data used to support the findings of this study are available from the corresponding author upon request.

Conflicts of Interest: The authors declare no conflict of interest.

References

1. Elseman, A.M.; Xu, C.; Yao, Y.; Elisabeth, M.; Niu, L.; Malavasi, L.; Song, Q.L. Electron transport materials: Evolution and case study for high-efficiency perovskite solar cells. *Sol. RRL* **2020**, *4*, 2000136. [CrossRef]
2. Huang, H.; Liu, X.; Duan, M.; Ji, J.; Jiang, H.; Liu, B.; Sajid, S.; Cui, P.; Wei, D.; Li, Y.; et al. Dual function of surface alkali-gas erosion on SnO₂ for efficient and stable perovskite solar cells. *ACS Appl. Energy Mater.* **2020**, *3*, 5039–5049. [CrossRef]
3. Shahiduzzaman; Fukaya, S.; Muslih, E.Y.; Wang, L.; Nakano, M.; Akhtaruzzaman; Karakawa, M.; Takahashi, K.; Nunzi, J.-M.; Taima, T. Metal oxide compact electron transport layer modification for efficient and stable perovskite solar cells. *Materials* **2020**, *13*, 2207. [CrossRef] [PubMed]
4. Ali, J.; Li, Y.; Gao, P.; Hao, T.; Song, J.; Zhang, Q.; Zhu, L.; Wang, J.; Feng, W.; Hu, H.; et al. Interfacial and structural modifications in perovskite solar cells. *Nanoscale* **2020**, *12*, 5719–5745. [CrossRef] [PubMed]
5. Nukunudompanich, M.; Budiutama, G.; Suzuki, K.; Hasegawa, K.; Ihara, M. Dominant effect of the grain size of the MAPbI₃ perovskite controlled by the surface roughness of TiO₂ on the performance of perovskite solar cells. *CrystEngComm* **2020**, *22*, 2718–2727. [CrossRef]
6. Nukunudompanich, M.; Budiutama, G.; Suzuki, K.; Hasegawa, K.; Ihara, M. Radio frequency magnetron sputtering deposition of TiO₂ thin films and their perovskite solar cell applications. *Sci. Rep.* **2016**, *5*, 17684.
7. Yang, W.S.; Park, B.-W.; Jung, E.H.; Jeon, N.J.; Kim, Y.C.; Lee, D.U.; Shin, S.S.; Seo, J.; Kim, E.K.; Noh, J.H.; et al. Iodide management in formamidinium-lead-halide-based perovskite layers for efficient solar cells. *Science* **2017**, *356*, 1376–1379. [CrossRef]
8. Yu, X.; Zou, X.; Cheng, J.; Chen, D.; Yao, Y.; Chang, C.; Liu, B.; Wang, J.; Zhou, Z.; Li, G. Investigation on low-temperature annealing process of solution-processed TiO₂ electron transport layer for flexible perovskite solar cell. *Materials* **2020**, *13*, 1031. [CrossRef]
9. Wang, J.; Zou, X.; Zhu, J.; Cheng, J.; Chen, D.; Bai, X.; Yao, Y.; Chang, C.; Yu, X.; Liu, B.; et al. Effect of optimization of TiO₂ electron transport layer on performance of perovskite solar cells with rough FTO substrates. *Materials* **2020**, *13*, 2272. [CrossRef]
10. Jiang, Q.; Zhao, Y.; Zhang, X.; Yang, X.; Chen, Y.; Chu, Z.; Ye, Q.; Li, X.; Yin, Z.; You, J. Surface passivation of perovskite film for efficient solar cells. *Nat. Photonics* **2019**, *13*, 460–466. [CrossRef]
11. Wang, Y.; Zhang, X.W.; Jiang, Q.; Liu, H.; Wang, D.; Meng, J.; You, J.; Yin, Z. Interface engineering of high-performance perovskite photodetectors based on PVP/SnO₂ electron transport layer. *ACS Appl. Mater. Interfaces* **2018**, *10*, 6505–6512. [CrossRef] [PubMed]
12. Jiang, Q.; Zhang, L.; Wang, H.; Yang, X.; Meng, J.; Liu, H.; Yin, Z.; Wu, J.; Zhang, X.; You, J. Enhanced electron extraction using SnO₂ for high-efficiency planar-structure HC(NH₂)₂PbI₃-based perovskite solar cells. *Nat. Energy* **2016**, *2*, 16177. [CrossRef]
13. Chen, J.; Dong, H.; Zhang, L.; Li, J.; Jia, F.; Jiao, B.; Xu, J.; Hou, X.; Liu, J.; Wu, Z. Graphitic carbon nitride doped SnO₂ enabling efficient perovskite solar cells exceeding 22%. *J. Mater. Chem. A* **2020**, *8*, 2644–2653. [CrossRef]

14. Zhang, W.; Ren, Z.; Guo, Y.; He, X.; Li, X. Improved the long-term air stability of ZnO-based perovskite solar cells prepared under ambient conditions via surface modification of the electron transport layer using an ionic liquid. *Electrochim. Acta* **2018**, *268*, 539–545. [[CrossRef](#)]
15. Son, D.Y.; Im, J.H.; Kim, H.S.; Park, N.G. 11% efficient perovskite solar cell based on ZnO nanorods: An effective charge collection system. *J. Phys. Chem. C* **2014**, *118*, 16567–16573. [[CrossRef](#)]
16. Mahmood, K.; Swain, B.S.; Kirmani, A.H.; Amassian, A. Highly efficient perovskite solar cells based on a nanostructured WO₃-TiO₂ core-shell electron transporting material. *J. Mater. Chem. A* **2015**, *3*, 9051–9057. [[CrossRef](#)]
17. Qin, M.; Ma, J.; Ke, W.; Qin, P.; Lei, H.; Tao, H.; Zheng, X.; Xiong, L.; Liu, Q.; Chen, Z.; et al. Perovskite solar cells based on low-temperature processed indium oxide electron selective layers. *ACS Appl. Mater. Interfaces* **2016**, *8*, 8460–8466. [[CrossRef](#)] [[PubMed](#)]
18. Kogo, A.; Numata, Y.; Ikegami, M.; Miyasaka, T. Nb₂O₅ blocking layer for high open-circuit voltage perovskite solar cells. *Chem. Lett.* **2015**, *44*, 829–830. [[CrossRef](#)]
19. Docampo, P.; Ball, J.M.; Darwich, M.; Eperon, G.E.; Snaith, H.J. Efficient organometal trihalide perovskite planar-heterojunction solar cells on flexible polymer substrates. *Nat. Commun.* **2013**, *4*, 1–6. [[CrossRef](#)] [[PubMed](#)]
20. Liu, D.; Kelly, T.L. Perovskite solar cells with a planar heterojunction structure prepared using room-temperature solution processing techniques. *Nat. Photonics* **2014**, *8*, 133–138. [[CrossRef](#)]
21. Yang, D.; Yang, R.; Wang, K.; Wu, C.; Zhu, X.; Feng, J.; Ren, X.; Fang, G.; Priya, S.; Liu, S.F. High efficiency planar-type perovskite solar cells with negligible hysteresis using EDTA-complexed SnO₂. *Nat. Commun.* **2018**, *9*, 3239. [[CrossRef](#)] [[PubMed](#)]
22. Giordano, F.; Abate, A.; Baena, J.P.C.; Saliba, M.; Matsui, T.; Im, S.H.; Zakeeruddin, S.M.; Nazeeruddin, M.K.; Hagfeldt, A.; Graetzel, M. Enhanced electronic properties in mesoporous TiO₂ via lithium doping for high-efficiency perovskite solar cells. *Nat. Commun.* **2016**, *7*, 10379. [[CrossRef](#)] [[PubMed](#)]
23. Ding, B.; Gao, L.; Liang, L.; Chu, Q.; Song, X.; Li, Y.; Yang, G.; Fan, B.; Wang, M.; Li, C.; et al. Facile and scalable fabrication of highly efficient lead iodide perovskite thin-film solar cells in air using gas pump method. *ACS Appl. Mater. Interfaces* **2016**, *8*, 20067. [[CrossRef](#)] [[PubMed](#)]
24. Calabrò, E.; Matteocci, F.; Palma, A.L.; Vesce, L.; Taheri, B.; Carlini, L.; Pis, I.; Nappini, S.; Dagar, J.; Battocchio, C.; et al. Low temperature, solution-processed perovskite solar cells and modules with an aperture area efficiency of 11%. *Sol. Energy Mater. Sol. Cells* **2018**, *185*, 136–144. [[CrossRef](#)]
25. Yang, Y.; Wu, J.; Guo, P.; Liu, X.; Guo, Q.; Liu, Q.; Luo, H. Low-temperature sintered SnO₂ electron transport layer for efficient planar perovskite solar cells. *J. Mater. Ence Mater. Electron.* **2018**, *29*, 13138–13147. [[CrossRef](#)]
26. Wang, H.; Zhu, C.; Liu, L.; Ma, S.; Liu, P.; Wu, J.; Shi, C.; Du, Q.; Hao, Y.; Xiang, S.; et al. Interfacial residual stress relaxation in perovskite solar cells with improved stability. *Adv. Mater.* **2019**, *31*, 1904408. [[CrossRef](#)]
27. Qiang, Y.; Cheng, J.; Qi, Y.; Shi, H.; Liu, H.; Geng, C.; Xie, Y. Low-temperature preparation of HTM-free SnO₂-based planar heterojunction perovskite solar cells with commercial carbon as counter electrode. *J. Alloy. Compd.* **2019**, *809*, 151817. [[CrossRef](#)]
28. Bahadur, J.; Ghahremani, A.H.; Martin, B.; Pishgar, S.; Druffel, T.; Sunkara, M.K.; Pal, K. A study on the material characteristics of low temperature cured SnO₂ flms for perovskite solar cells under high humidity. *J. Mater. Sci. Mater. Electron.* **2019**, *30*, 18452–18461. [[CrossRef](#)]
29. Bu, T.; Li, J.; Zheng, F.; Chen, W.; Wen, X.; Ku, Z.; Peng, Y.; Zhong, J.; Cheng, Y.-B.; Huang, F. Universal passivation strategy to slot-die printed SnO₂ for hysteresis-free efficient flexible perovskite solar module. *Nat. Commun.* **2018**, *9*, 4609. [[CrossRef](#)]
30. Huang, K.; Peng, Y.; Gao, Y.; Shi, J.; Li, H.; Mo, X.; Huang, H.; Gao, Y.; Ding, L.; Yang, J. High-performance flexible perovskite solar cells via precise control of electron transport layer. *Adv. Energy Mater.* **2019**, *9*, 44. [[CrossRef](#)]
31. Chen, Y.; Meng, Q.; Xiao, Y.; Zhang, X.; Sun, J.; Han, C.; Gao, H.; Zhang, Y.; Lu, Y.; Yan, H. Mechanism of PbI₂ situ-passivated perovskite films for enhancing performance of perovskite solar cells. *ASC Appl. Mater. Inter.* **2019**, *11*, 44101–44108. [[CrossRef](#)] [[PubMed](#)]